Front. Chem. Sci. Eng. 2019, 13(3): 485–492
https://doi.org/10.1007/s11705-019-1831-2

RESEARCH ARTICLE

Improvement in growth yield of single-walled carbon nanotubes with narrow chirality distribution by pulse plasma CVD

Bin Xu[1], Toshiro Kaneko[1], Toshiaki Kato (✉)[1,2]

1 Department of Electronic Engineering, Tohoku University, Sendai 980-8579, Japan
2 Japan Science and Technology Agency (JST)-PRESTO, Sendai 980-8579, Japan

Abstract A pulse plasma chemical vapor deposition (CVD) technique was developed for improving the growth yield of single-walled carbon nanotubes (SWNTs) with a narrow chirality distribution. The growth yield of the SWNTs could be improved by repetitive short duration pulse plasma CVD, while maintaining the initial narrow chirality distribution. Detailed growth dynamics is discussed based on a systematic investigation by changing the pulse parameters. The growth of SWNTs with a narrow chirality distribution could be controlled by the difference in the nucleation time required using catalysts comprising relatively small or large particles as the key factor. The nucleation can be controlled by adjusting the pulse on/off time ratio and the total processing time.

Keywords single-walled carbon nanotubes, chirality-controlled synthesis, pulse plasma chemical vapor deposition

1 Introduction

Owing to their excellent electrical and optical properties, single-walled carbon nanotubes (SWNTs) [1,2] are expected to be utilized in a wide range of applications such as in thin film transistors, photodetectors in the THz range, and chemical sensors [3–5]. Over the last two decades, the selective growth of SWNTs with specific chirality, which determines the physical and chemical properties of the SWNTs such as their bandgap, carrier mobility, quantum yield, and chemical reactivity, has been regarded as a critical issue. Owing to the recent progress in the catalyzed growth of SWNTs, significant improvements in the control of their chirality have been achieved, leading to the fabrication of SWNTs with a narrow chirality distribution. Using various kinds of catalysts, such as bi-metallic catalysts comprising Co and Mo (CoMoCAT), SWNTs with (6,5), (7,5), and (7,6) chirality can be grown preferentially [6]. The addition of a small amount of impurities such as Mn and Cr to Co can result in the formation of (6,5) dominant SWNTs [7,8]. Au-catalyzed growth with hydrogen-assisted plasma chemical vapor deposition (CVD) can lead to the preferential formation of (6,5) SWNTs [9]. On mixing S with Co, (9,8) SWNTs can be obtained [10]. SWNTs with (14,10) and (15,8) chirality and a relatively large diameter (d) can be grown predominantly using Rh catalysts [11]. The highly crystalline $Co_xMg_{1-x}O$ catalyst can furnish (6,5), (7,6), and (9,4) SWNTs [12]. W-based bi-metallic alloy catalysts maintain their crystalline structures during nucleation, and catalyze the formation of (12,6), (14,4), and (16,0) SWNTs with high selectivity [13–15]. Recently, our group developed a novel chirality-controlled method based on controlling the surface state of the catalyst for the growth of SWNTs. By controlling the degree of oxidation of the surface of a Co catalyst, we accomplished the preferential synthesis of (6,4) SWNTs for the first time [16]. The aforementioned studies were mainly focused on controlling the catalyst. By controlling the morphology and chemical component of the catalyst, the dominant chirality of the SWNT could be determined. To further tune the chiral species among the dominant chiralities towards achieving a narrow chirality distribution, studies on the CVD process are carried out. Elemental parameters such as the CVD temperature [17,18] and gas sources [19] are found to influence the diameter distribution of the SWNTs. The CVD pressure, which changes the carbon supply, also influences the chirality distribution of SWNTs [20]. Some novel studies

Received August 31, 2018; accepted February 17, 2019

E-mail: kato12@ecei.tohoku.ac.jp

have shown that the chirality of SWNTs can be controlled by controlling the charge transfer as well [21]. Our group has reported the growth of SWNTs with a narrow chirality distribution by controlling the gas phase reaction using very short duration (~few seconds) plasma CVD (Fig. 1(a)). Thereby, small-diameter SWNTs were preferentially nucleated, resulting in the predominant growth of (7,6) and (8,4) SWNTs [22]. This technique is based on the concept of nucleation dynamics, where smaller catalyst particles preferentially nucleate faster than the larger ones, owing to the difference in the incubation time. This approach is useful for obtaining SWNT species with specific chirality. However, the amount of SWNTs that can be grown in a single experiment is very small because of the short growth time.

These recent progresses in the synthesis of SWNTs with selective chirality have furnished materials for fundamental studies. Thus, the synthesis of SWNTs should move to the next stage, which is how to use these chirality-selective SWNTs in practical devices. For this purpose, it is very important to achieve large-scale synthesis of SWNTs with a specific chirality. Thus, it is imperative to develop a method that can increase the growth yield of SWNTs while the high chiral selectivity is maintained.

To address this issue, in this study, we extend the specific time-scale gas-phase reaction-controlled method for scaling up the production of SWNTs with a narrow chirality distribution. In the proposed method, short-duration plasma CVD, termed as pulse plasma CVD, is employed with multiple repetitions. This can increase the amount of SWNTs grown while maintaining the original narrow chirality distribution. We also investigate the mechanism of the growth of SWNTs during the pulse plasma CVD, revealing that the initially nucleated SWNTs continuously grow in the axial direction with repetitive pulse plasma cycles. This novel approach is promising for the high-yield synthesis of SWNTs with a narrow chirality distribution.

2 Materials and methods

A custom-made plasma CVD system was used for diffusion plasma CVD, which is the same apparatus used in our former research [23]. Before growing the SWNTs by plasma CVD, an electric furnace was heated to the desired temperature (center area of the electric furnace was typically at ~600°C). When furnace reached the desired temperature, CH_4 (20 sccm; 32 Pa) was flown into it. The catalyst holder was then immediately transferred to the central area of the furnace and heated rapidly. When the catalyst holder was heated to the growth temperature, the pressure was adjusted to 60 Pa. Afterwards, radio frequency power of 28 W (13.56 MHz) was supplied to the coils outside the quartz tube to generate the CH_4 plasma in the plasma generation zone located 45 cm away from the center of the furnace. A typical plasma irradiation time of 2 min was employed. After plasma CVD, the power supply to the furnace was turned off, which led to the drop in the temperature of the catalyst holder. When the temperature of the catalyst holder decreased to 500°C, the supply of CH_4 gas was discontinued and the substrate was removed from the central area of the electrical furnace. The sample was taken out when the temperature of the catalyst holder dropped below 100°C.

Two types of catalysts were used in this study. For Raman mapping, a thin Co film deposited on a SiO_2/Si substrate was used as the catalyst. For the photoluminescence excitation (PLE) measurement, a zeolite-supported Co (CoMo) catalyst [24,25] was used. This catalyst was

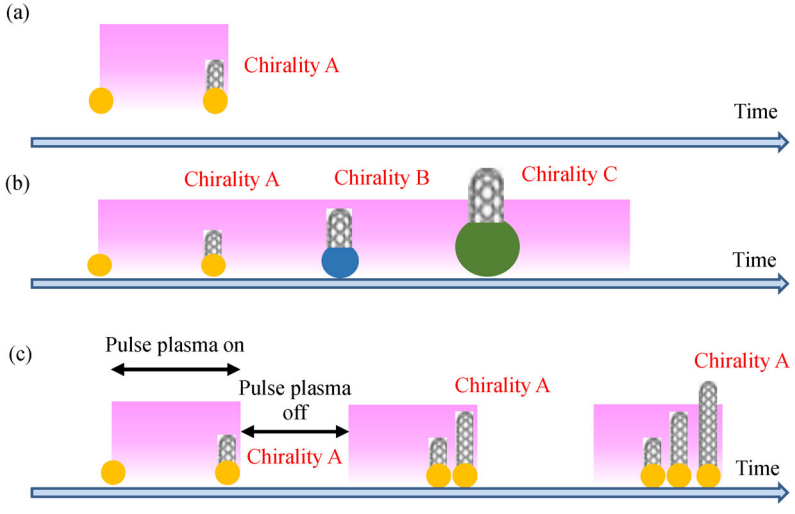

Fig. 1 (a,b) Model for the growth of SWNTs with (a) long and (b) short growth times; (c) Imaging model of SWNT growth using the new pulse plasma CVD method.

prepared as follows: first, 0.5 wt-% acetate tetrahydrate (or 0.5 wt-% acetate dimer) was mixed with ferrierite zeolite (1 g). Then, the prepared solid catalyst was dispersed in 20 mL ethanol through ultrasonication for 15 min. After that, it was heated at 80°C for 24 h under atmospheric conditions.

The prepared SWNT samples and catalysts were characterized by scanning electron microscopy (SEM; SU-70, Hitachi, Japan), atomic force microscopy (AFM; JSPM-5400, JEOL, Japan), and Raman scattering spectroscopy [26] (HR-800, Horiba, Japan) using 488 nm Ar laser and 632 nm He-Ne laser excitation sources. The chirality of the SWNTs was evaluated via UV-vis-NIR spectroscopy (V-7200HK, JASCO, Japan) and PLE mapping [27,28] (NanoLog, Horiba, Japan). A 450 W Xe lamp emitting in the 500–800 nm range was used as the excitation light in 4 nm steps. The photoluminescence (PL) spectra were recorded using a liquid-nitrogen-cooled InGaAs array detector in the 900–1400 nm range at room temperature. The slit width used for emission and excitation was 10 nm. The length of the SWNTs was estimated from AFM images. For this, the SWNTs were dispersed in sodium cholate deuterium oxide solution using an ultrasonic homogenizer. Then, a Si substrate was soaked in the solution, rinsed with water, and dried. Tapping mode AFM was used to acquire images of the SWNTs on the Si substrate under ambient conditions.

3 Results and discussion

3.1 Growth of SWNTs with narrow chirality distribution by pulse plasma CVD

Repetitive Raman mapping was used to identify the effect of pulse plasma CVD on the structural distribution of the SWNTs. Here, we used exactly the same substrate and same position in order to monitor the temporal evolution of the SWNT structures as a function of the pulse parameters. One pulse was fixed at 5 s on and 20 s off. Figures 2(a–f) show the Raman mapping, that is, the intensity of the G-band (I_G) as a function of repetitive pulse plasma CVD up to 24 times. Before the pulse plasma CVD process, a marker was placed on the growing substrate, which enabled repeated measurement at the same spot. Because I_G is linearly proportional to the graphitic area within the laser spot, I_G can be used as a parameter for monitoring the growth yield. Note that all Raman measurements were carried out under the same measurement conditions (i.e., using the same laser power, accumulation time, and mapping resolution). The I_G gradually increased with repetitive pulse plasma CVD, indicating that SWNT growth continued even after multiple repetitions of the pulse plasma CVD. The intensity of the D-band (I_D) did not change with repeated pulse cycles, indicating the quality of the SWNTs grown by this pulse plasma CVD to

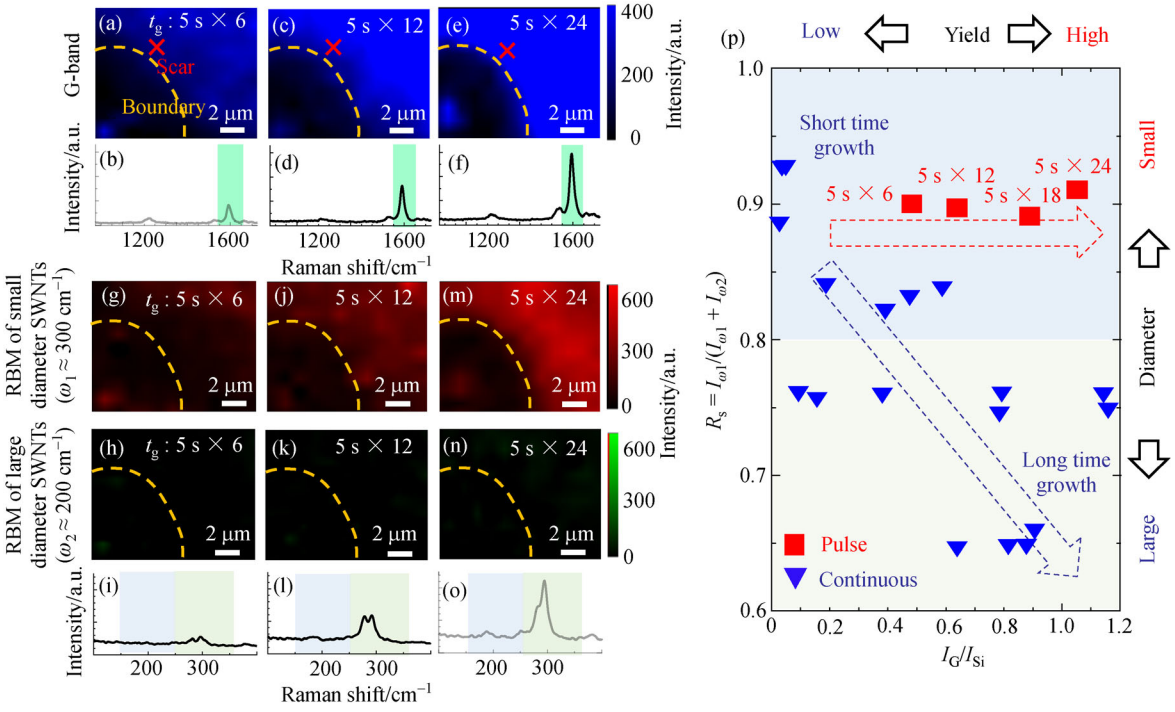

Fig. 2 (a–o) Raman measurement of SWNT growth with 6, 12, and 24 pulse repetitions; (a–c) G-band mapping; (b–f) corresponding Raman spectrum is marked in the map using a red cross; (i–o) RBM mapping at wavelengths of 300 cm^{-1} (g–m) and 200 cm^{-1} (h–n), and the corresponding RBM; (p) Yield and diameter distribution of SWNTs synthesized by pulse plasma CVD and continuous plasma CVD based on Raman measurement.

be as high as that of SWNTs grown by conventional CVD [29]. The Raman mapping data were analyzed in different Raman modes. The radial breathing mode (RBM) (ω), ranging from 100 to 400 cm^{-1}, provides information on the diameter (d) of the SWNTs ($\omega \approx 248/d$). Two different RBMs ($\omega_1 \approx 300$ cm^{-1} and $\omega_2 \approx 200$ cm^{-1}) were selected to represent the small and large diameters, respectively. Mapping of the intensity of the ω_1 mode ($I_{\omega 1}$) revealed that the intensity increased with repetitive CVD pulses, implying that the small-diameter SWNTs grew continuously with repeated pulse plasma CVD. Conversely, mapping of the intensity of the ω_2 ($I_{\omega 2}$) mode showed almost negligible changes in the peak even after 24 repetitions. This indicates that the relatively large-diameter SWNTs did not grow with this repeated pulse plasma CVD sequence. These results are compared with those of continuous plasma CVD (Fig. 1(b)). Here, we introduced R_s as an indicator of the concentration of small-diameter SWNTs, which is defined as follows: $R_s = I_{\omega 1} / (I_{\omega 1} + I_{\omega 2})$. The ratio of I_G normalized relative to the intensity of the signal from the Si substrate (I_{Si}) (I_G/I_{Si}) increased with the growth time for continuous CVD, whereas R_s decreased with the growth time. This result suggests that not only small-diameter SWNTs, but also the large-diameter SWNTs could grow with the continuous plasma CVD. Thus, R_s remained high and I_G/I_{Si} increased with repeated pulses during the pulse plasma CVD, as deduced by the Raman maps. The Raman mapping data confirm that pulse plasma CVD can increase the yield of the SWNTs while maintaining the initial good selectivity in the growth of small-diameter SWNTs, leading to the growth of SWNTs with both narrow chirality distribution and high yield, which is as expected.

For a more comprehensive evaluation of the chirality distribution of the SWNTs during the repetitive pulse growth process, PLE measurements were carried out on SWNTs grown with different numbers of pulse repetitions. The PLE signal remained unchanged when the number of repeated pulses was increased from 3 (Fig. 3(a)) to 15 (Fig. 3(b)). This result indicates that the chirality of the SWNTs remained unchanged, which may be due to the continual growth of the initially grown small-diameter SWNTs. Note that since SWNTs used for Raman and PL measurement were grown on different substrates (plane SiO_2 and powder zeolite), the chirality distributions determined by Raman and PLE measurements are slightly different.

3.2 Dynamics of the nucleation of SWNTs during the pulse plasma CVD

To further narrow the chirality distribution, it is important to focus on the following critical questions: (1) why does the growth yield increase with repeated pulse plasma cycles? and (2) why does the chirality distribution become narrow upon introducing pulse plasma? In order to answer the first question, the length distribution of the SWNTs grown with different numbers of pulse repetitions was determined by AFM (Figs. 4(a–c)). Initially, when three pulse repetitions were used, only short SWNTs (under 100 nm) were generated (Fig. 4(d)). However, when further pulses were applied to the sample, the number of initial short SWNTs decreased, whereas the number of long SWNTs increased (Figs. 4(e) and (f)). With an increase in the number of pulses from 3 to 15, the length distribution of the SWNTs continued to increase. The average length of the SWNTs was calculated as a function of the pulse repetitions (Fig. 4(g)), indicating that the average length increased linearly in proportion to the number of pulse repetitions, while the chirality of the SWNTs remained almost unchanged (Figs. 3(a) and (b)). These results indicate that during repeated pulses, further growth of the SWNTs formed in the initial pulse may be the predominant growth mode, which is in good accordance with our imaging growth model in Fig. 1(c) and might be the answer to question (1).

The chirality distribution of the SWNTs generated using different pulse parameters was also investigated to address

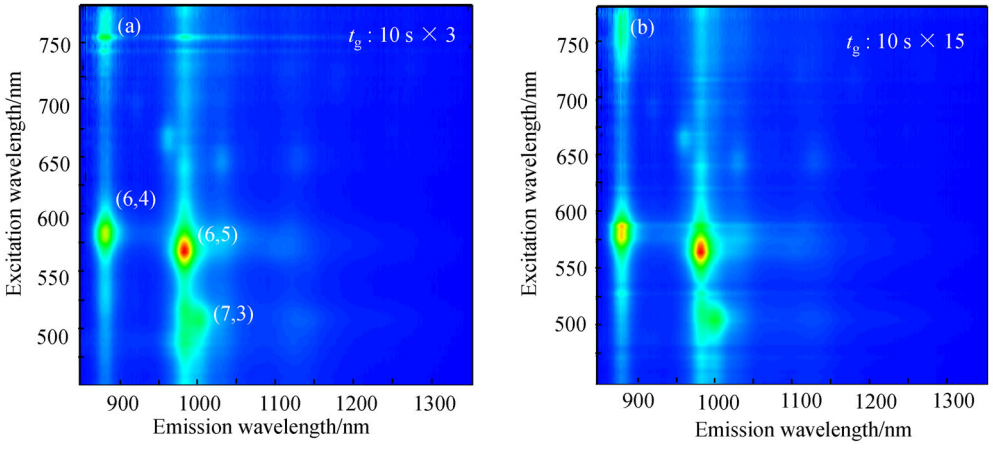

Fig. 3 PLE mapping of SWNTs grown with different number of pulse repetitions. (a) 10 s × 3 times and (b) 15 times.

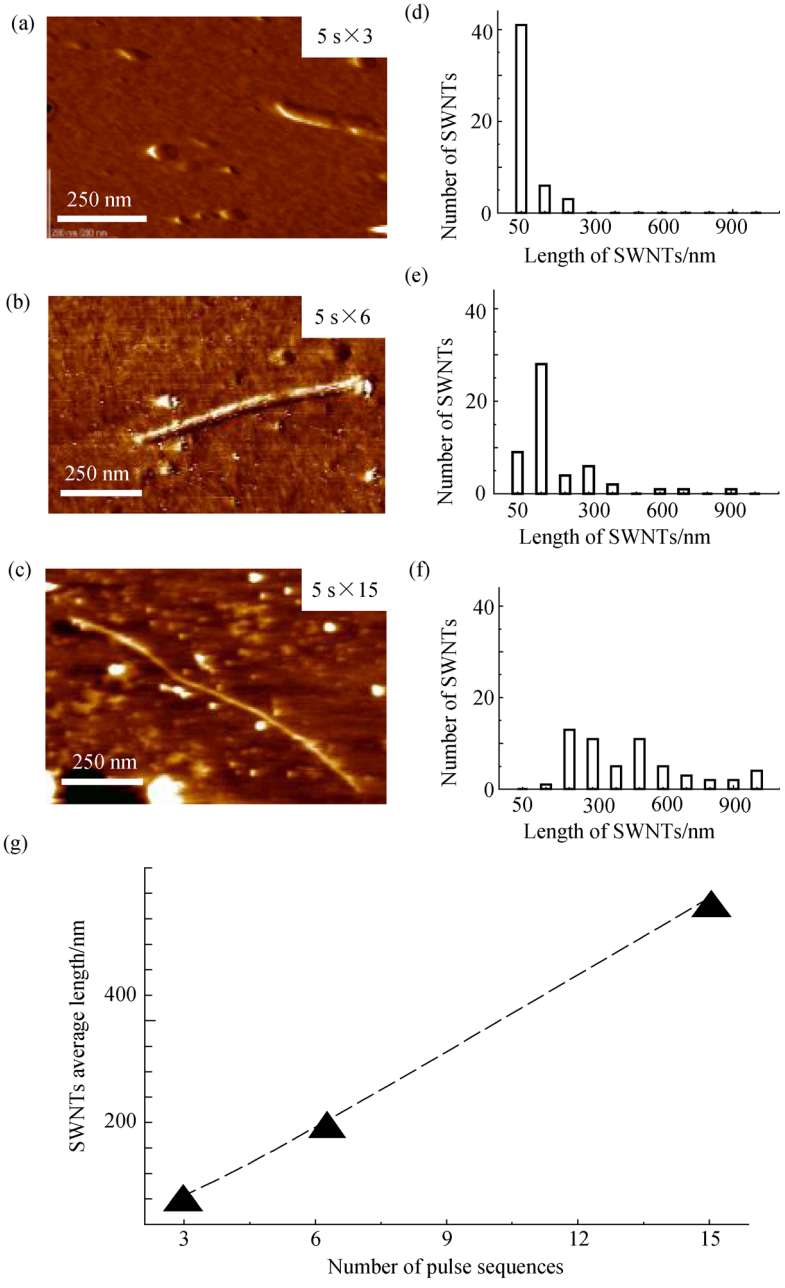

Fig. 4 (a–c) AFM image and (d–f) histogram of the length of SWNTs grown with different pulse repetitions: (a,d) 3, (b,e) 6, and (c,f) 15 times; (g) Average SWNT length as a function of number of pulse repetitions.

question (2) (Fig. 5(a)). For this experiment, the total 'on' time was kept constant at 120 s. The chirality did not vary monotonously when the pulse 'on' time was changed (off time = 30 s). However, the chirality distribution became narrower (broader) with an increase (decrease) in the pulse 'on' time in regions (i) & (ii). A similar two-phase variation of the SWNT chirality distribution was also observed as a function of the pulse 'off' time (on time = 5 s) (Fig. 5(b)). In region (i) ($0\ s < t_{off} < 30\ s$), the chirality distribution became narrower with an increase in the pulse 'off' time, whereas in region (ii) ($30\ s < t_{off}$), the chirality distribution became broader with an increase in the pulse 'off' time. The chirality distributions of the SWNTs synthesized using various pulse 'on' and 'off' time sets are plotted in Fig. 5(c). Note that the chirality distribution was evaluated based on 1/e time the width of the diameter distribution obtained from the PLE map (Figs. 5(a) and (b)). A narrow chirality distribution could be obtained within a limited time region (II) that can be expressed in terms of the pulse on/off time ratio (t_{on}/t_{off}), corresponding to the range, $0.06 < t_{on}/t_{off} < 0.18$.

To identify the critical meaning of the lower threshold

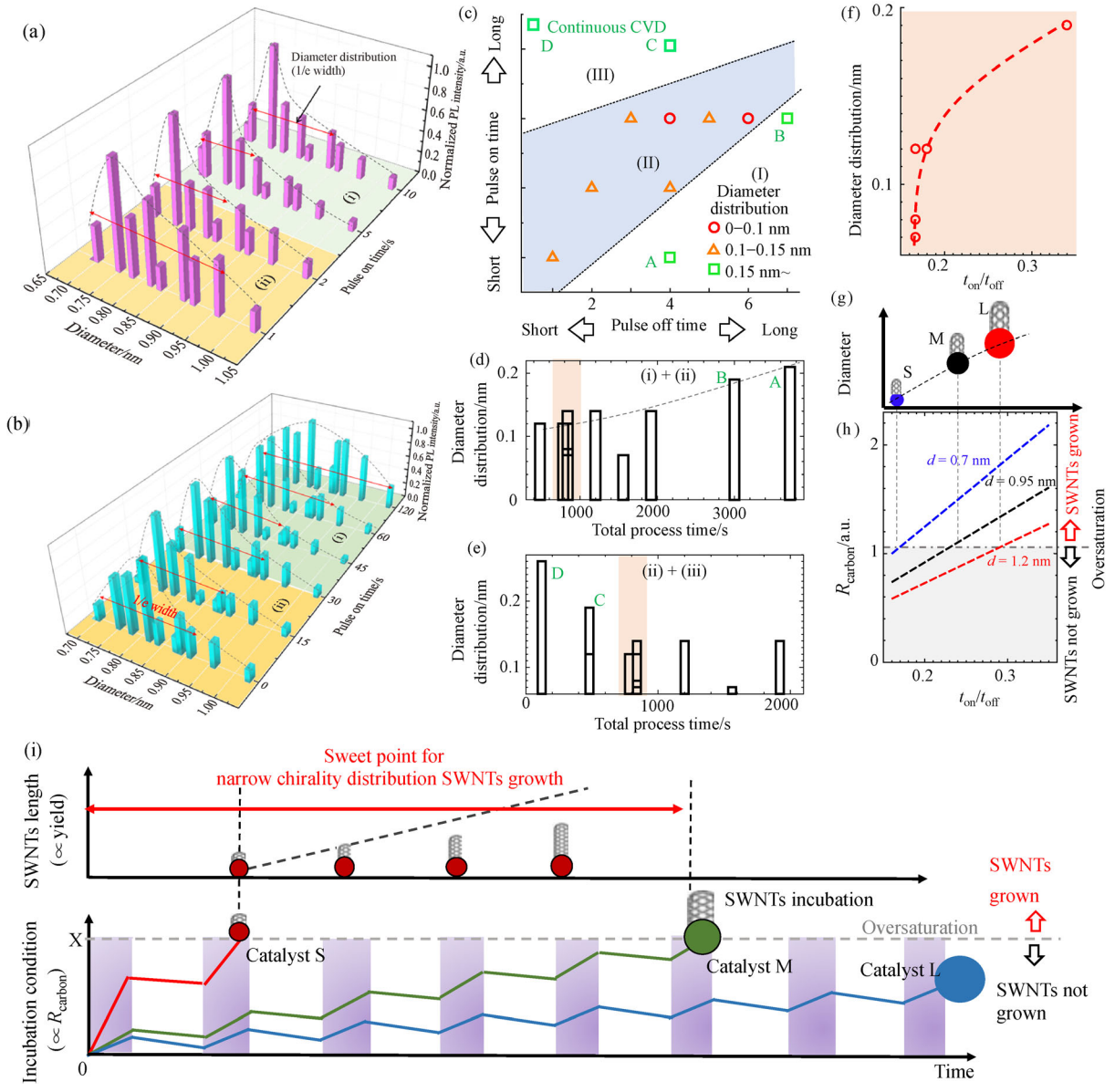

Fig. 5 Diameter distribution vs. pulse (a) on time with the off time fixed and (b) off time with the on time fixed; (c) diameter distribution vs. different pulse on and off times; (a–e) diameter distribution vs. total process time; (f) diameter distribution vs. pulse on/off time ratio; (a–f) are derived from PLE mapping data; (g–h) Calculated carbon dissolution rate vs. pulse on/off time ratio.

($0.06 > t_{on}/t_{off}$), the data were replotted as a function of the total process time. A clear trend is observed, where the diameter distribution became broad with an increase in the total process time. A longer total process time can promote aggregation of the catalyst [30,31], resulting in the growth of large-diameter SWNTs. A similar plot was obtained for the higher threshold region. With an increase in the total process time, no broadening of the SWNT diameter distribution was observed, implying that aggregation is less important in this region, allowing for a more meaningful discussion of the influence of the pulse parameters on the incubation dynamics. To further eliminate the influence of catalyst aggregation, the data obtained using a relatively short process time were selected, where the total process time was approximately 800 s (indicated as the orange zone in Figs. 5(d) and (e)). Because the pulse on/off time ratio (t_{on}/t_{off}) was already proven to be a critical factor influencing the chirality distribution, as shown in Fig. 5(c), we plotted the data as a function of t_{on}/t_{off} (Fig. 5(f)). With an increase in t_{on}/t_{off}, the chirality distribution became broader, implying that t_{on}/t_{off} is a determinant of the chirality distribution. To explain this result, we trace back to the SWNT incubation model [22]. This model provides a detailed description of the critical conditions for SWNT lift-off, where the SWNTs can only be detached when the catalyst is oversaturated with carbon:

$$R_{\text{carbon}} > X, \tag{1}$$

where, R_{carbon} is the percentage of carbon atoms dissolved into the catalyst and X is the carbon dissolution ratio fulfilling the threshold condition for lift-off of the SWNTs. To clarify the trend in Fig. 5(f), we calculated R_{carbon} for different pulse on/off ratios, as shown in Fig. 5(f). We assumed that the carbon dissolution rate is only influenced by the plasma and carbon feedstock conditions, and the quantity of carbon that dissolves into the catalyst is proportional to the carbon dissolution time, which is the effective total pulse 'on' time. Thus, R_{carbon} can be calculated according to the following equation:

$$R_{\text{carbon}} = \frac{V_C' \times R_{\text{Time}} \times t_{\text{Total}}}{\frac{4}{3}\pi\left(\frac{d}{2}\right)^3}. \tag{2}$$

The V_C' for different catalysts of different diameters can be calculated as:

$$V_C' = 4\pi\left(\frac{d}{2}\right)^2 \times V_C, \tag{3}$$

where, R_{Time}, V_C , V_C', t_{Total}, and d are the pulse on/off time ratio, carbon adsorption speed per unit area, total carbon adsorption speed for one catalyst, total process time, and catalyst diameter, respectively. The different diameters and different on and off time parameters from Fig. 5(f) were substituted into Eqs. (2) and (3), and R_{carbon} was plotted as a function of these parameters (Fig. 5(h)). When the total process time was fixed at 800 s, R_{carbon} was proportional to the pulse on/off time ratio. The increase in R_{carbon} with time was inversely proportional to the catalyst diameter. To achieve the critical carbon ratio in the catalyst for the lift-off of the SWNTs, larger catalyst particles ($d \approx 1.2$ nm) require a higher on/off time ratio, whereas smaller catalyst particles ($d \approx 0.7$ nm) require a much lower pulse on/off time ratio (Fig. 5(g)). The calculated data are in good accordance with the experimental results in Fig. 5(h), where a smaller on/off ratio results in a narrow diameter distribution.

Overall, the incubation dynamics before lift-off of the SWNTs can be summarized as follows: (1) the initially formed short SWNTs with narrow chirality distribution continue to grow during repeated pulses (Fig. 5(i)); (2) the growth of large-diameter SWNTs is suppressed by the repetition of the pulse off sequence (Fig. 5(i)).

4 Conclusions

SWNTs with a narrow chirality distribution were successfully grown in a relatively high yield by developing a new pulse plasma CVD method that facilitated improved control over the SWNT incubation dynamics. Based on the systematic study of the influence of the pulse time, temporal variation in the length of the SWNTs, and incubation dynamics of the SWNTs during pulse plasma CVD, we demonstrated that the growth of large-diameter SWNTs is suppressed during repeated pulse off sequences, while the initially formed short SWNTs with narrow chirality distribution continue to grow during the repeated pulse on sequences. This study on the precise time-scale incubation dynamics controlling the growth of SWNTs during pulse plasma CVD offers novel insights for the development of chirality-controlled SWNTs.

Acknowledgements This work was supported in part by the Grant-in-Aid for Scientific Research B (Grant No. 16H03892), Grant-in-Aid for Challenging Exploratory Research (Grant No. 16K13707) from JSPS KAKENHI, JST-PRESTO (Grant No. J170002074), and the Cooperative Research Project Program of the Research Institute of Electrical Communication, Tohoku University.

References

1. Ueda A, Matsuda K, Tayagaki T, Kanemitsu Y. Carrier multiplication in carbon nanotubes studied by femtosecond pump-probe spectroscopy. Applied Physics Letters, 2008, 92(23): 233105
2. Javey A, Guo J, Wang Q, Lundstrom M, Dai H. Ballistic carbon nanotube field-effect transistors. Nature, 2003, 424(6949): 654–657
3. Qiu C, Zhang Z, Xiao M, Yang Y, Zhong D, Peng L M. Scaling carbon nanotube complementary transistors to 5-nm gate lengths. Science, 2017, 355(6322): 271–276
4. He X, Fujimura N, Lloyd J M, Erickson K J, Talin A A, Zhang Q, Gao W, Jiang Q, Kawano Y, Hauge R H, et al. Carbon nanotube terahertz detector. Nano Letters, 2014, 14(7): 3953–3958
5. Kim H S, Kim W J, Strano M S, Han J H. Optical detection of argon gas flow based on vibration-induced change in photoluminescence of a semiconducting single-walled carbon nanotube bundle. Journal of Nanoscience and Nanotechnology, 2014, 14(12): 9131–9133
6. Lolli G, Zhang L, Balzano L, Sakulchaicharoen N, Tan Y, Resasco D E. Tailoring (*n*,*m*) structure of single-walled carbon nanotubes by modifying reaction conditions and the nature of the support of CoMo catalysts. Journal of Physical Chemistry B, 2006, 110(5): 2108–2115
7. Loebick C Z, Derrouiche S, Marinkovic N, Wang C, Hennrich F, Kappes M M, Haller G L, Pfefferle L D. Effect of manganese addition to the Co-MCM-41 catalyst in the selective synthesis of single wall carbon nanotubes. Journal of Physical Chemistry C, 2009, 113(52): 21611–21620
8. Loebick C Z, Derrouiche S, Fang F, Li N, Haller G L, Pfefferle L D. Effect of chromium addition to the Co-MCM-41 catalyst in the synthesis of single wall carbon nanotubes. Applied Catalysis A, General, 2009, 368(1-2): 40–49
9. Ghorannevis Z, Kato T, Kaneko T, Hatakeyama R. Narrow-chirality distributed single-walled carbon nanotube growth from nonmagnetic catalyst. Journal of the American Chemical Society, 2010, 132 (28): 9570–9572
10. Zhang L, Hou P, Li S, Shi C, Cong H, Liu C, Cheng H. *In situ* TEM observations on the sulfur-assisted catalytic growth of single-wall

carbon nanotubes. Journal of Physical Chemistry Letters, 2014, 5 (8): 1427–1432

11. Li P, Zhang X, Liu J. Aligned single-walled carbon nanotube arrays from rhodium catalysts with unexpected diameter uniformity independent of the catalyst size and growth temperature. Chemistry of Materials, 2016, 28(3): 870–875
12. He M, Jiang H, Kauppi I, Fedotov P V, Chernov A I, Obraztsova E D, Cavalca F, Wagner J B, Hansen T W, Sainio J, et al. Insights into chirality distributions of single-walled carbon nanotubes grown on different $Co_xMg_{1-x}O$ solid solutions. Journal of Materials Chemistry. A, Materials for Energy and Sustainability, 2014, 2(16): 5883–5889
13. Yang F, Wang X, Zhang D, Yang J, Luo D, Xu Z, Peng F, Li X, Li R, Li Y, et al. Chirality-specific growth of single-walled carbon nanotubes on solid alloy catalysts. Nature, 2014, 510(7506): 522–524
14. Yang F, Wang X, Si J, Zhao X, Qi K, Jin C, Zhang Z, Li M, Zhang D, Yang J, et al. Water-assisted preparation of high-purity semiconducting (14,4) carbon nanotubes. ACS Nano, 2017, 11(1): 186–193
15. Yang F, Wang X, Zhang D, Qi K, Yang J, Xu Z, Li M, Zhao X, Bai X, Li Y. Growing zigzag (16,0) carbon nanotubes with structure-defined catalysts. Journal of the American Chemical Society, 2015, 137(27): 8688–8691
16. Xu B, Kaneko T, Shibuta Y, Kato T. Preferential synthesis of (6,4) single-walled carbon nanotubes by controlling oxidation degree of Co catalyst. Scientific Reports, 2017, 7(11149): 1–9
17. He M, Fedotov P V, Chernov A, Obraztsova E D, Jiang H, Wei N, Cui H, Sainio J, Zhang W, Jin H, et al. Chiral-selective growth of single-walled carbon nanotubes on Fe-based catalysts using CO as carbon source. Carbon, 2016, 108: 521–528
18. Rao R, Pierce N, Liptak D, Hooper D, Sargent G, Semiatin S L, Curtarolo S, Harutyunyan A R, Maruyama B. Revealing the impact of catalyst phase transition on carbon nanotube growth by *in situ* Raman spectroscopy. ACS Nano, 2013, 7(2): 1100–1107
19. Wang B, Poa C H P, Wei L, Li L, Yang Y, Chen Y. (*n*,*m*) Selectivity of single-walled carbon nanotubes by different carbon precursors on Co-Mo catalysts. Journal of the American Chemical Society, 2007, 129(29): 9014–9019
20. Picher M, Anglaret E, Arenal R, Jourdain V. Processes controlling the diameter distribution of single-walled carbon nanotubes during catalytic chemical vapor deposition. ACS Nano, 2011, 5(3): 2118–2125
21. Wang J, Liu P, Xia B, Wei H, Wei Y, Wu Y, Liu K, Zhang L, Wang J, Li Q, et al. Observation of charge generation and transfer during CVD growth of carbon nanotubes. Nano Letters, 2016, 16(7): 4102–4109
22. Kato T, Hatakeyama R. Direct growth of short single-walled carbon nanotubes with narrow-chirality distribution by time-programmed plasma chemical vapor deposition. ACS Nano, 2010, 4(12): 7395–7400
23. Xu B, Kato T, Murakoshi K, Kaneko T. Effect of ion impact on incubation time of single-walled carbon nanotubes grown by plasma chemical vapor deposition. Plasma and Fusion Research, 2014, 9: 1206075-1-3
24. Maruyama S, Kojima R, Miyauchi Y, Chiashi S, Kohno M. Low-temperature synthesis of high-purity single-walled carbon nanotubes from alcohol. Chemical Physics Letters, 2002, 360(3-4): 229–234
25. Kato T, Jeong G H, Hirata T, Hatakeyama R. Structure control of carbon nanotubes using radio-frequency plasma enhanced chemical vapor deposition. Thin Solid Films, 2004, 457(1): 2–6
26. Shiau S H, Liu C W, Gau C, Dai B T. Growth of a single-wall carbon nanotube film and its patterning as an *n*-type field effect transistor device using an integrated circuit compatible process. Nanotechnology, 2008, 19(10): 105303
27. O'Connell M J, Bachilo S M, Huffman C B, Moore V C, Strano M S, Haroz E H, Rialon K L, Boul P J, Noon W H, Kittrell C, et al. Band gap fluorescence from individual single-walled carbon nanotubes. Science, 2002, 297(5581): 593–596
28. Weisman R B, Bachilo S M. Dependence of optical transition energies on structure for single-walled carbon nanotubes in aqueous suspension: An empirical Kataura plot. Nano Letters, 2003, 3(9): 1235–1238
29. Hou B, Wu C, Inoue T, Chiashi S, Xiang R, Maruyama S. Extended alcohol catalytic chemical vapor deposition for efficient growth of single-walled carbon nanotubes thinner than (6,5). Carbon, 2017, 119: 502–510
30. Ostrikov K, Mehdipour H. Thin single-walled carbon nanotubes with narrow chirality distribution: Constructive interplay of plasma and Gibbs-Thomson effects. ACS Nano, 2011, 5(10): 8372–8382
31. Lifshitz I, Slyozov V. The kinetics of precipitation from supersaturated solid solutions. Journal of Physics and Chemistry of Solids, 1961, 19(1-2): 35–50